

See discussions, stats, and author profiles for this publication at: <https://www.researchgate.net/publication/237066026>

Binding of Pt Nanoclusters to Point Defects in Graphene: Adsorption, Morphology, and Electronic Structure

DATASET in THE JOURNAL OF PHYSICAL CHEMISTRY C · FEBRUARY 2012

Impact Factor: 4.77 · DOI: 10.1021/jp2110117

CITATIONS

65

READS

1,636

2 AUTHORS, INCLUDING:



[Ioanna Fampiou](#)

University of Delaware

9 PUBLICATIONS 96 CITATIONS

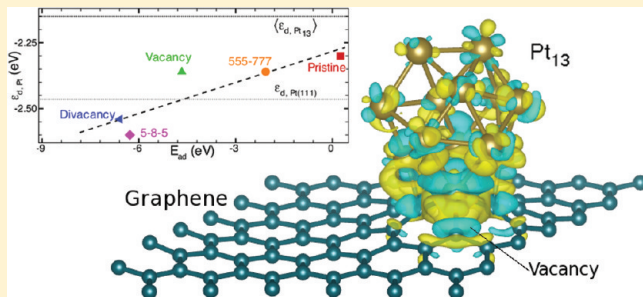
[SEE PROFILE](#)

Binding of Pt Nanoclusters to Point Defects in Graphene: Adsorption, Morphology, and Electronic Structure

Ioanna Fampiou and Ashwin Ramasubramaniam*

Department of Mechanical and Industrial Engineering, University of Massachusetts, Amherst, Massachusetts 01003, United States

ABSTRACT: Graphene nanosheets serve as excellent support materials in the synthesis of advanced metal nanoparticle–graphene electrocatalysts. In this study, we employ a combination of density functional theory and bond-order potential calculations to perform a systematic investigation of the adsorption energetics, structural features, and electronic structure of platinum nanoclusters supported on both defective and defect-free graphene. We establish a hierarchy of point defects and their reconstructions that can act as strong trapping sites for platinum nanoclusters and inhibit catalyst sintering. We demonstrate that the preferred low-energy structure of supported platinum nanoclusters are neither high-symmetry structures (e.g., icosahedral, cuboctahedral) nor readily derived from moderate structural distortions of high-symmetry structures, as is often assumed in computational models. Rather, supported nanoparticles assume open, low-symmetry shapes much like those observed in earlier computational work on annealing of unsupported clusters in a vacuum. The formation of metal–carbon bonds at support defects influences the average bond length and thus the strain in the metal cluster, stronger binding correlating with larger average bond lengths. Additionally, stronger binding of the cluster to the support leads to increased charge transfer from the cluster to the substrate accompanied by a substantial downshift of the cluster d-band center; in several instances, the d-band center is shifted below that of a Pt(111) surface. Our study suggests possible avenues for enhancing the stability and CO tolerance of platinum nanoparticles on graphene through defect engineering.



I. INTRODUCTION

Carbonaceous materials such as activated carbon and carbon black¹ and, more recently, nanostructured forms of carbon such as nanotubes² and graphite nanofibers³ are widely used as catalyst supports because of their high surface areas, excellent electrical conductivity, resistance to corrosion, and structural stability. Carbon nanotubes, for example, exhibit greater stability and are better at suppressing catalyst aggregation than traditional carbon black supports.⁴ More recently, a spate of advances in synthesizing graphene-based nanomaterials have opened up exciting avenues for the development of graphene-supported metal catalysts.^{5–9} Preliminary experiments already indicate much promise for platinum–graphene nanocomposites as electrocatalysts in direct methanol fuel cells,^{5,6} proton-exchange membrane fuel cells (for oxygen reduction),⁷ and hydrogen fuel cells.⁸ Compared with standard Pt–carbon black catalysts, Pt–graphene composites display enhanced catalytic activity and tolerance to CO poisoning,^{5,6} as well as long-term stability toward sintering,^{5–7} with typical stable cluster sizes remaining below 5 nm. Moreover, these experiments have also demonstrated facile solution-processing methods for the preparation of these catalyst materials. Thus, the overall outlook for Pt–graphene catalysts in transportation and portable electronics applications appears promising.

Pristine graphene is an sp^2 -bonded carbon allotrope and is relatively inert. Metal clusters are typically weakly adsorbed on

graphene and can diffuse fairly easily along the surface,^{10,11} leading to eventual catalyst sintering. Therefore, despite its desirable properties such as excellent electrical conductivity and structural stability, pristine graphene is unlikely to be a suitable support unless appropriate strategies can be devised to stabilize and immobilize clusters. Defect engineering of graphene is one such possibility with promise; intuition suggests that under-coordinated C atoms should act as traps for metal atoms. Indeed, experiments clearly reveal that electron-damage-induced point defects in graphene are very effective traps for diffusing atoms and clusters.¹² This was also noted in older work on highly oriented pyrolytic graphite (HOPG) surfaces by Zoval et al.,¹³ who demonstrated that Pt nanoparticles nucleate preferentially at point defects and step edges on the graphite basal plane. Such defect-mediated anchoring of Pt nanoparticles is also expected to prevail in experimentally synthesized Pt–graphene composites, which are typically produced through solution processing of graphene oxide. Graphene oxide is known to contain lattice defects (vacancies, holes) and functional groups (carboxyls, epoxides, hydroxyls, etc.)^{14–16} that can act as strong anchoring sites for Pt nanoparticles;^{7,17,18} this could explain the increased stability of Pt nanoparticles toward sintering in these composites.

Received: November 15, 2011

Revised: February 26, 2012

Published: February 26, 2012



Other strategies such as boron^{19–21} or nitrogen²¹ doping have also been proposed for enhancing the binding of Pt clusters to graphene.

From a computational perspective, the interaction of Pt clusters with graphene and carbon nanotubes has been extensively researched; a representative, but by no means exhaustive, list includes refs 17, 18, 22–24, and 27–36. Briefly, the following features of Pt–graphene interactions can be gleaned from these studies. First, Pt does not wet pristine graphene because of the relatively high cohesive energy for Pt as compared to the Pt–C bond energy.^{23,24,34} Consequently, Pt clusters on graphene are essentially three-dimensional structures for cluster sizes in excess of about ten atoms. Second, Pt clusters bind more strongly to defects (vacancies,³⁰ disclinations,²⁹ dopants,²² edges,^{18,28} 5-8-5 reconstructed divacancies¹⁷) in graphene because of the formation of strong Pt–C bonds at the defect, which partially alleviates the disruption of the graphene sp² network. The electronic structure of the cluster is modified both through bond formation and through strains induced in the cluster. Third, there is a clear indication of charge transfer from the Pt cluster to the graphene support, accompanied by a shift of the Pt d band away from the Fermi level that is greater in the presence of a support defect.^{29–31,36} The binding energy of CO molecules, for example, is found to decrease as one goes from an unsupported particle, to a supported one, to one on a defective support;²⁹ this provides a plausible explanation for the increased CO tolerance of Pt–graphene nanocomposites. Similarly, the presence of vacancies in the graphene substrate has been shown to enhance the stability of Pt₁₃ nanoparticles on the graphene support while weakening the O₂ adsorption energy on the cluster; this effect can alter the catalytic activity of the nanoparticle toward oxygen reduction.³⁶ The presence of a defect on the graphene support was also found to increase the reactivity of Pt₄ clusters and reduce the barrier of catalyzed CO oxidation.³⁷

Several studies on the adsorption and electronic properties of clusters of various other metals on graphene have also been performed. Logsdail and Akola³⁸ investigated the adsorption of Au₁₆ nanoclusters on bilayer graphene with varying numbers of defects and different cluster orientations and found that the adsorption energy increases with the number of the defects, leading to distortion of the initial structure. The cluster binds to the top layer of graphene, creating Au–C bonds of metallic nature. The same authors also found that, in the presence of defects, O₂ binding to the Au₁₆ nanocluster was unfavorable in most cases. Lim et al.³⁹ studied the structural and electronic properties of graphene-supported Fe₁₃ and Al₁₃ nanoparticles and found strong binding at vacancies, which they attributed to significant hybridization between the metal cluster with the sp² dangling bonds of the carbon atoms. Recently, Liu et al.⁴⁰ investigated the properties of Pd nanoparticles on defective graphene as oxygen reduction catalysts. They found increased binding energy of Pd₁₃ nanoclusters at vacancies and hybridization of the dsp states of Pd with the sp² dangling bonds of carbon, accompanied by a shift of the d-band center of the Pd nanoparticles away from the Fermi level. The defective graphene support was found to reduce the adsorption energies of O, OH, and OOH on the Pd₁₃ nanoparticles, which is directly related to electrocatalytic performance in oxygen reduction reactions.

The goal of this work is to provide a systematic investigation of the structural and electronic properties of Pt clusters in relation to the type of substrate defect that binds the cluster.

Specifically, we are interested in the hierarchy of the energetics of binding of Pt_{*n*} (*n* = 1–4, 13) clusters to pristine graphene, vacancies, unreconstructed divacancies, pentagon-octagon-pentagon (5-8-5) reconstructed divacancies, and haecelite (555-777) reconstructed divacancies in graphene. Divacancies are of particular interest as they present the smallest defect in graphene with nontrivial reconstructions, namely, the 5-8-5 and 555-777 reconstructions.^{41,42} Apart from binding energetics of specific cluster geometries, we are also interested in identifying low-energy isomers of these clusters and the possible correlation between the structure of a Pt_{*n*} cluster and the type of binding defect. These substrate-induced structural modifications are expected to influence the electronic structure and activity of the cluster. Such low-energy structures have been identified fairly systematically for small Pt clusters on pristine graphene and at vacancies;^{24,34} comparisons to the existing literature are presented in section III. To the best of our knowledge, no systematic studies at divacancies and reconstructed divacancies have been performed. At best, there have been investigations of binding of a Pt₆ cluster¹⁷ and a Pt₂₇ cluster¹⁸ to a 5-8-5 defect; however, neither study appears to have undertaken a systematic optimization of the cluster shape beyond structural relaxations starting from a specific initial guess. Indeed, this appears to be the prevalent situation even in other studies of binding of Pt₁₃ clusters to pristine graphene and to vacancy defects wherein the clusters have typically been assumed to be of icosahedral (*I*_h) symmetry prior to relaxation.^{27,29,31} Okazaki-Maeda et al.²⁴ used a few other initial guesses such as icosahedral, cuboctahedral (*O*_h), planar, and layered Pt₁₃ clusters in their study of binding to pristine graphene; although a bias from initial conditions is still to be expected, their study nevertheless provides more insight into the classes of low-energy structures that might be expected. Also, although structural relaxation can certainly induce significant distortions in the cluster shape, typical relaxation algorithms (steepest descent, conjugate gradient, etc.) are guaranteed only to find local minima in the vicinity of the initial guess rather than a global minimum. Furthermore, although there is still some debate about the minimum-energy structures even for unsupported clusters, density functional theory studies^{45–48} clearly indicate that Pt₁₃ clusters tend to adopt low-symmetry, open structures rather than high-symmetry compact ones; the latter (*I*_h, *O*_h symmetries) can be about 2 eV higher in energy than their low-symmetry counterparts. Hence, we suggest that studies of high-symmetry supported clusters—even after structural relaxation—might not convey meaningful information about the electronic structure and activity of realistic Pt clusters. To address this issue in more detail, we study both relaxed high-symmetry supported clusters (on a variety of substrate defects) and low-symmetry clusters generated by molecular dynamics (MD) annealing and demonstrate that the annealed structures are significantly more stable than the relaxed high-symmetry ones. Finally, we also present a detailed electronic structure analysis of Pt₁₃ clusters bound at various defects and correlate cluster–substrate charge transfer and cluster d-band shifts with the strength of binding to the defect.

The remainder of this article is organized as follows: In section II, we present computational details of our calculations. Results and discussion of cluster binding energetics, structural analyses, and electronic structures are presented in section III. Concluding remarks are provided in section IV.

II. COMPUTATIONAL DETAILS

In this study, we employed a combination of density functional theory (DFT) and empirical potential (EP) simulations at the level of Tersoff–Brenner potentials. EP simulations allow for extended molecular dynamics (MD) annealing runs and sampling to generate candidate low-symmetry structures for further DFT studies, as described in detail below. We present the details of the DFT calculations first, followed by those of the EP calculations.

DFT calculations were performed using the Vienna Ab Initio simulation package (VASP).⁴⁹ The projector-augmented-wave (PAW) method^{50,51} was used to describe the core and valence electrons; the PAW potentials were derived from fully relativistic atomic calculations. The Perdew–Burke–Ernzerhof⁵² form of the Generalized-Gradient Approximation was employed to describe electron exchange and correlation. All calculations were performed on a 6×6 graphene supercell (72 atoms) with periodic boundary conditions; periodic images were separated by 18 Å of vacuum normal to the sheets to prevent spurious image interactions. A kinetic energy cutoff of 400 eV was used in all simulations, and the Brillouin zone was sampled using a $5 \times 5 \times 1$ Γ -centered k -point mesh. Structural relaxations were performed using a conjugate gradient algorithm until forces on all atoms were below 0.01 eV/Å. To accelerate electronic convergence, a second-order Methfessel-Paxton⁵³ smearing of the Fermi surface was employed with a smearing width of 0.05 eV. All calculations were spin-polarized. For isolated Pt clusters, calculations were performed in a large supercell with Γ -point sampling only.

EP calculations were performed using the LAMMPS simulation package⁵⁴ with a Tersoff–Brenner-style potential for Pt–C developed by Albe et al.⁵⁵ The EP calculations were performed for the same 72-atom graphene sheet that was used in the entire set of the DFT calculations; the only difference of note was that the graphene supercell employed in this case was constructed at the equilibrium C–C bond length of 1.45 Å for the Tersoff–Brenner potential as opposed to the DFT value of 1.42 Å. Structural relaxations, analogous to those in the DFT studies, were performed with conjugate gradient minimization and a tolerance of 10^{-4} eV/Å on the N -dimensional force vector. In addition to structural relaxation, supported 13-atom Pt clusters on the various defective graphene substrates were also subjected to MD annealing in a canonical (NVT) ensemble. For these annealing studies, the system was initially thermalized at 1500 K for 50 ps and gradually cooled to 1 K over an additional 50 ps. Structural data were then gathered over 2.5 ps at 1 K. The MD time step was set to 1 fs. The system was then reheated to 1500 K, and the annealing process was repeated. This entire heat–anneal–gather procedure was repeated eight times to allow the system to sample the energy landscape more extensively and to gather reasonable statistics. The lowest-energy structures were then imported into VASP for further structural relaxation and electronic structure analysis; the lattice vectors and atomic positions were rescaled in this step to account for the slight mismatch of the EP (1.45 Å) and DFT (1.42 Å) C–C bond lengths. This procedure allowed us to generate low-symmetry, low-energy structures at minimal computational cost that could then be studied in greater detail with DFT. Of course, it is entirely possible that the EP potential energy surface is quite different from the DFT one, which implies that an optimal EP structure might not be close to optimal in DFT. Also, there is no guarantee that annealing brings the system close to a global minimum. Nevertheless, as demonstrated later,

this procedure was sufficient to identify structures that were favored by several electronvolts over those obtained from structural relaxation of high-symmetry shapes alone.

Regarding Pt clusters, for high-symmetry structures, we considered the Pt monomer, dimer, linear and triangular Pt trimers, planar and tetrahedral Pt tetramers, and I_h and O_h Pt₁₃ clusters. The DFT-optimized vacuum structures for Pt₃, Pt₄, and Pt₁₃ clusters are displayed in Figure 1. For substrates, we

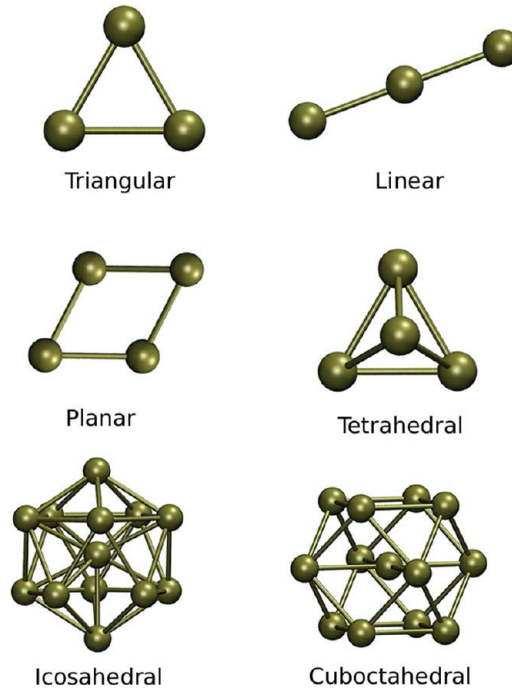


Figure 1. DFT-optimized cluster geometries in vacuum for linear and triangular Pt₃ clusters, planar and tetrahedral Pt₄ clusters, and icosahedral (I_h) and cuboctahedral (O_h) Pt₁₃ clusters.

considered pristine (defect-free) graphene and defective graphene with a single vacancy, an unreconstructed divacancy, a 5-8-5 reconstructed divacancy, and a 555-777 reconstructed divacancy, which are displayed in Figure 2.

For both DFT and EP calculations, we report the adsorption energy, E_{ad} , and the formation energy, E_f , of the clusters. The adsorption energy, E_{ad} , of a Pt _{n} cluster is defined as

$$E_{ad} = E_{C_m+Pt_n} - E_{C_m} - E_{Pt_n} \quad (1)$$

where $E_{C_m+Pt_n}$, E_{C_m} , and E_{Pt_n} are the total energies of the Pt _{n} –graphene system, the graphene sheet of m carbon atoms, and the Pt _{n} cluster in vacuum, respectively. The formation energy is defined as

$$E_f = E_{C_m+Pt_n} - mE_C - nE_{Pt} \quad (2)$$

where $E_{C_m+Pt_n}$ is the total energy of the Pt _{n} –graphene system and E_C and E_{Pt} are the energies of a C atom in graphene and a Pt atom in vacuum, respectively. As defined, a more negative value of E_{ad} signifies stronger binding of a cluster to the support. Similarly, a more negative value of E_f signifies greater thermodynamic stability of the structure with respect to the reference states of its individual constituents. For adsorption energy calculations, the reference energy of each Pt _{n} ($n = 1–4$) cluster was taken to be that of its corresponding high-symmetry structure (Figure 1) in vacuum. Supported Pt₁₃ clusters can

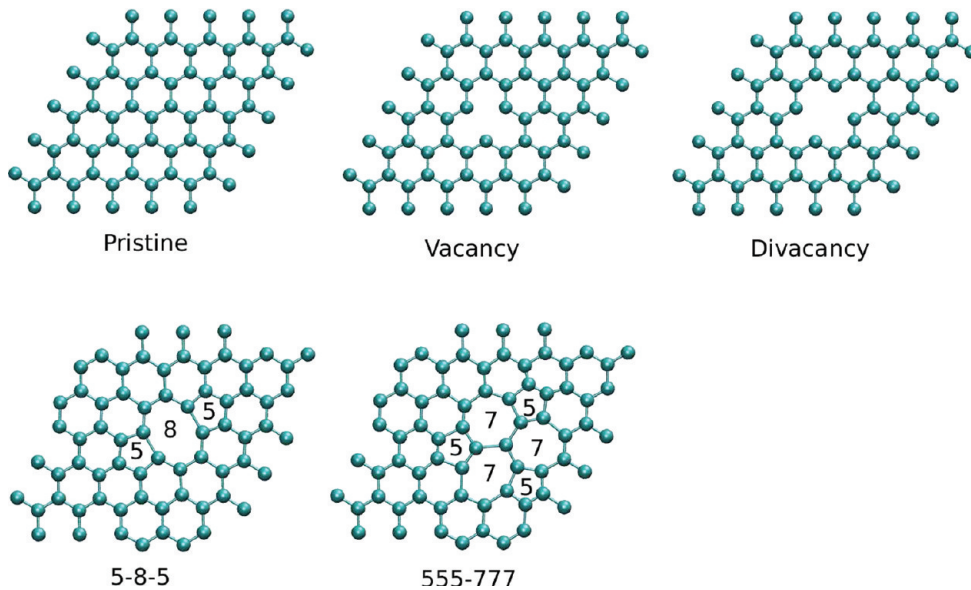


Figure 2. Defect-free and defective graphene substrates employed in this study. Pentagons, heptagons, and octagons associated with divacancy reconstructions are indicated.

often display final relaxed shapes that are significantly different from their high-symmetry vacuum structures (even though the latter represents the initial condition for relaxation). For low-symmetry Pt_{13} clusters generated by MD annealing on the graphene support, there is no correlation whatsoever with the high-symmetry vacuum structures. Therefore, there is some ambiguity in defining the reference energy of the Pt_{13} cluster in the adsorption energy calculation. We employed the simple strategy of removing the carbon atoms from the fully relaxed/annealed Pt-graphene structure and relaxing the residual Pt cluster alone in vacuum. This cluster energy was then chosen as the reference for computing the adsorption energy; this definition is not unique, and other equally valid choices could have been made. The formation energy clearly does not suffer from any such ambiguities.

III. RESULTS AND DISCUSSION

III.A. Adsorption of Pt Atoms. First, we examine the adsorption of a single Pt atom on the five different graphene substrates. In each case, there are several stable adsorption sites (hollow/top/bridge sites) that can be rendered inequivalent through substrate reconstructions. For brevity, we report adsorption and formation energies along with C–Pt bond lengths only for minimum-energy structures in Table 1; corresponding atomic structures (from DFT) are displayed in Figure 3. On pristine graphene, a single Pt atom is adsorbed most strongly on the bridge site (B site), which is consistent with several previous studies,^{24–26,31,33,34} and it is located 1.97 Å above the graphene layer. This result is in good agreement with the values reported by Błoński et al.³⁴ and Okazaki-Maeda et al.²⁴ At a vacancy, the Pt atom essentially binds as a substitutional atom that is displaced by 1.12 Å out of the graphene plane because of the greater length of a C–Pt bond as compared to a C–C bond. At an unreconstructed divacancy, the Pt atom occupies a “cross” configuration and is again slightly displaced out of the graphene plane by 0.31 Å. These observations are in agreement with DFT calculations by Krasheninnikov et al.⁵⁶ Also, as noted by those authors, our DFT results also confirm that the Pt atom is bound less strongly to the divacancy because

Table 1. Optimal Adsorption Energies, Formation Energies, and C–Pt Bond Lengths ($d_{\text{C–Pt}}$) for Single Pt Atom on Pristine Graphene, Single Vacancy, Unreconstructed Divacancy, 5-8-5 Reconstructed Divacancy, and 555-777 Reconstructed Divacancy^a

substrate	E_{ad} (eV)	E_f (eV)	$d_{\text{C–Pt}}$ (Å)
pristine	-1.57 (-1.99)	-1.57 (-1.99)	2.10 (2.06)
vacancy	-7.45 (-6.68)	0.54 (-1.37)	1.94 (1.98)
divacancy	-6.97 (-8.60)	0.71 (-1.51)	1.98 (2.01)
5-8-5	-6.12 (-6.94)	0.71 (-1.51)	1.99 (2.01)
555-777	-2.38 (-2.27)	4.71 (2.28)	2.06 (2.07)

^aEP values are in parentheses.

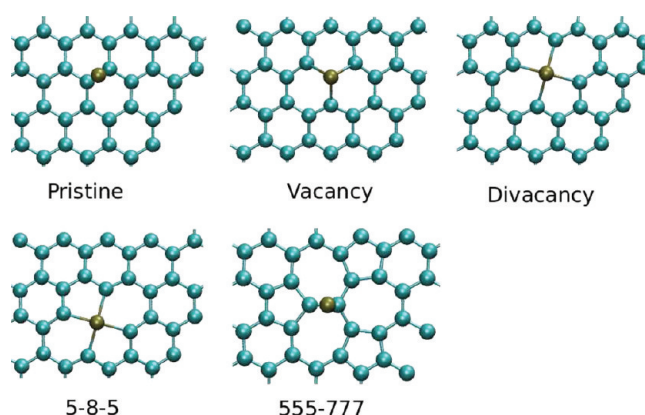


Figure 3. Low-energy DFT configurations for adsorption of a Pt atom on graphene. Cyan and gold spheres represent C and Pt atoms, respectively.

of weaker interactions with the ligand bonds. This is not reflected in the EP calculation, however, which predicts that the Pt atom binds more strongly to the divacancy than the vacancy.⁶¹ The 5-8-5 and 555-777 defects bind the Pt atom more weakly than the unreconstructed divacancy but more strongly than pristine graphene. Interestingly, the unreconstructed divacancy and 5-8-5 structures in Figure 3 produced identical adsorption

Table 2. Optimal Adsorption Energies, Formation Energies, C–Pt Bond Lengths (d_{C-Pt}), and Pt–Pt Bond Lengths (d_{Pt-Pt}) for Pt Dimers on Pristine Graphene, Single Vacancy, Unreconstructed Divacancy, 5-8-5 Reconstructed Divacancy, and 555-777 Reconstructed Divacancy^a

substrate	E_{ad} (eV)	E_f (eV)	d_{C-Pt} (Å)	d_{Pt-Pt} (Å)
pristine	−0.78 (−1.94)	−4.58 (−5.62)	2.25 (2.07)	2.38 (2.39)
vacancy	−7.26 (−6.93)	−3.07 (−5.30)	1.96, 2.01 (1.96, 1.97)	2.53 (2.63)
divacancy	−6.40 (−8.66)	−2.52 (−5.25)	1.97, 2.04 (1.96, 2.01)	2.56 (2.72)
5-8-5	−4.14 (−7.34)	−1.11 (−5.58)	1.92, 2.00 (1.94)	2.51 (2.62)
555-777	−2.43 (−2.21)	0.86 (−1.35)	2.07 (2.07)	2.33 (2.39)

^aEP values in parentheses.

configurations after the DFT calculations, even though the initial configurations of the graphene sheet were different (unreconstructed versus reconstructed). The Pt atom thus appears to break the 5-8-5 reconstruction. This was not observed for the 555-777 substrate case, which is known to be a lower-energy (more stable) reconstruction than the 5-8-5 defect^{41,42} and is therefore less prone to unreconstructing. Finally, an examination of the formation energies shows that, with the exception of the pristine sheet, the defective sheets with adsorbed Pt atoms are all thermodynamically less stable than their constituents. This is a reflection of the high defect formation energy in each case, which is not adequately compensated by the formation of bonds with the single Pt atom.

III.B. Adsorption of Pt Dimers. Next, we consider adsorption of a Pt_2 cluster (dimer) on defect-free and defective graphene substrates. We report adsorption and formation energies only for the lowest-energy structures in Table 2 and their corresponding atomic structures (from DFT) in Figure 4.

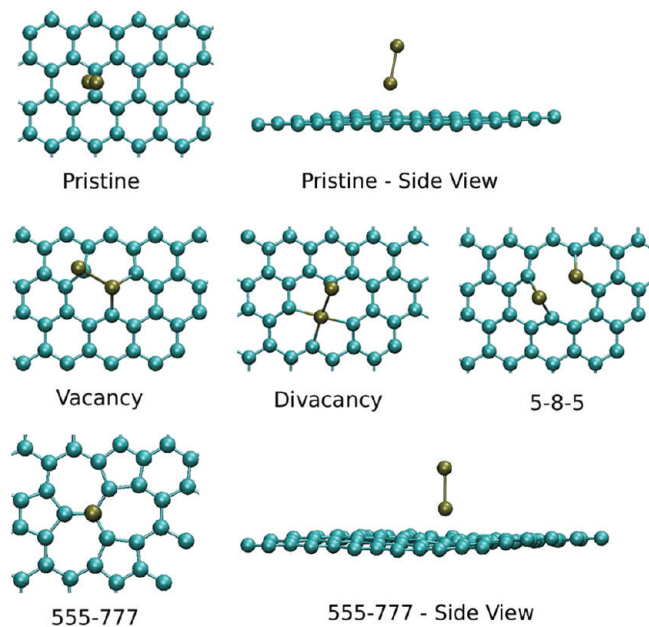


Figure 4. Low-energy DFT configurations for Pt dimers on graphene. Cyan and gold spheres represent C and Pt atoms, respectively.

For pristine graphene, we found that the most stable configuration is a vertically oriented dimer bound at a bridge site. The Pt–Pt (DFT) bond length for the adsorbed dimer is elongated to 2.38 Å as compared to the gas-phase bond length of 2.33 Å. These results are in agreement with the study by Bloński and Hafner;³⁴ the horizontal adsorption configuration

(Pt atoms bound at diametrically opposite near-on-top sites of the hexagon), which was predicted to be the lowest-energy structure by Okazaki-Maeda et al.,²⁴ is actually adsorbed less weakly by 0.36 eV as compared to the vertical dimer.

For adsorption at a vacancy or divacancy, one Pt atom is consistently bound at an on-top site (slightly displaced) whereas the second Pt atom occupies a position similar to that occupied by a single Pt atom bound at the defect (substitutional/cross configuration displaced out of the graphene plane; see section III.A). The dimer is bound more strongly to the single vacancy than to the unreconstructed divacancy, as was the case for Pt_1 . Similarly, the 5-8-5 and 555-777 defects bind the dimer more strongly than pristine graphene but less strongly than either the vacancy or the divacancy. For the 5-8-5 case, we observed, as in the case of the single Pt atom, that the dimer breaks the reconstruction; the Pt atoms are situated at bridge sites of atoms shared by the pentagon and octagon. Clearly, this is a local minimum en route to the dimer–divacancy configuration. The empirical potential once again reverses the relative ordering of adsorption energies at the vacancy and divacancy in comparison with DFT. For adsorption at the 555-777 defect, the most stable configuration is similar to the one we found for the pristine graphene case and consists of a vertically oriented dimer bound at the bridge site between the pentagon and heptagon of the 555-777 defect. It is interesting to note that, in the cases in which there are no dangling bonds (pristine and 555-777 substrate), the most stable adsorption configuration is the upright dimer, whereas for the other three substrates, the dimer binds to the substrate in a manner that passivates the dangling C bonds. Thermodynamically, all structures with the exception of the 555-777 case are stable with respect to their individual components.

III.C. Adsorption of Pt Trimers. The Pt_3 cluster (trimer) has two nonequivalent structures, namely, the linear and triangular configurations shown in Figure 1. We considered adsorption of these two structures both parallel and perpendicular to the graphene substrates. Adsorption and formation energies for the most stable structures and average Pt–C and Pt–Pt bond lengths are reported in Table 3, and the corresponding atomic structures (from DFT) are displayed in Figure 5. In none of the cases is the linear trimer chain energetically preferred. For pristine graphene, we found that the triangular configuration with two Pt atoms bound to the substrate was the most stable one, in agreement with other studies.^{24,34} The basal Pt atoms are bound to the substrate at positions intermediate between on-top and bridge sites, in agreement with ref 34 and in disagreement with ref 24, which seems to favor bridge sites. At a vacancy, one atom at the vertex of the triangle is bound at the site of the missing C atom with an out-of-plane displacement as before; the second Pt atom occupies a bridge site; the third Pt atom is directly bonded only to the Pt atoms. At a divacancy, two Pt atoms of the cluster passivate the dangling C bonds; the third Pt atom is bound only

Table 3. Optimal Adsorption Energies, Formation Energies, Average C–Pt Bond Lengths ($\langle d \rangle_{C-Pt}$), and Average Pt–Pt Bond Lengths ($\langle d \rangle_{Pt-Pt}$) for Pt Trimers on Pristine Graphene, Single Vacancy, Unreconstructed Divacancy, 5-8-5 Reconstructed Divacancy, and 555-777 Reconstructed Divacancy^a

substrate	E_{ad} (eV)	E_f (eV)	$\langle d \rangle_{C-Pt}$ (Å)	$\langle d \rangle_{Pt-Pt}$ (Å)
pristine	-1.35 (-2.54)	-8.64 (-10.06)	2.22 (2.06)	2.49 (2.61)
vacancy	-7.61 (-6.52)	-6.91 (-8.73)	1.96 (2.02)	2.54 (2.59)
divacancy	-6.33 (-7.95)	-5.94 (-8.38)	1.96 (2.01)	2.48 (2.64)
5-8-5	-5.54 (-7.50)	-6.00 (-9.59)	2.05 (1.99)	2.57 (2.73)
555-777	-5.15 (-2.05)	-5.34 (-5.02)	2.04 (2.07)	2.50 (2.50)

^aEP values are in parentheses.

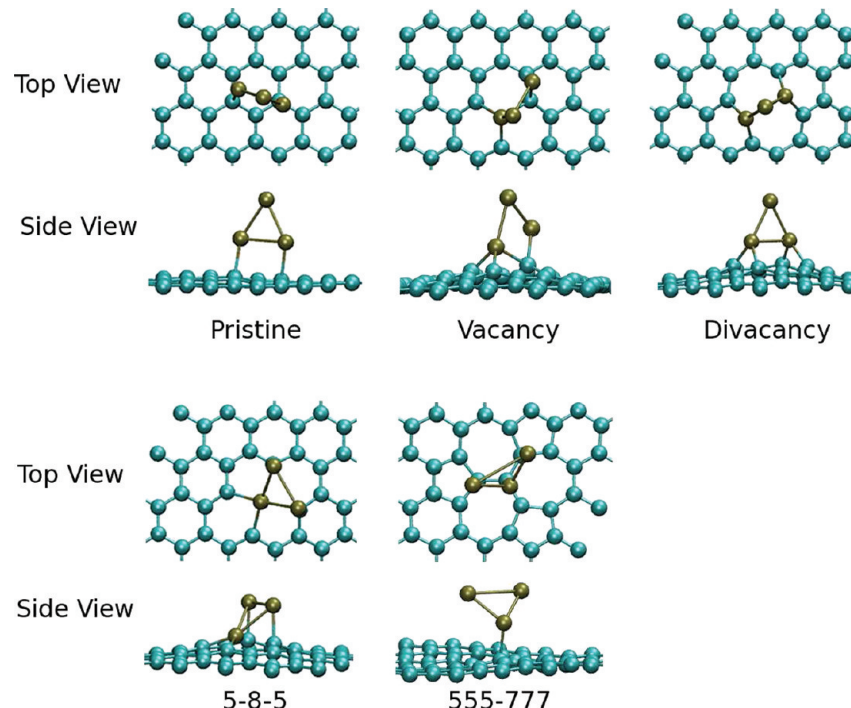


Figure 5. Low-energy DFT configurations for Pt trimers on graphene. Cyan and gold spheres represent C and Pt atoms, respectively.

Table 4. Optimal Adsorption Energies, Formation Energies, Average C–Pt Bond Lengths ($\langle d \rangle_{C-Pt}$), and Average Pt–Pt Bond Lengths ($\langle d \rangle_{Pt-Pt}$) for Pt Tetramers on Pristine Graphene, Single Vacancy, Unreconstructed Divacancy, 5-8-5 Reconstructed Divacancy, and 555-777 Reconstructed Divacancy^a

substrate	E_{ad} (eV)	E_f (eV)	$\langle d \rangle_{C-Pt}$ (Å)	$\langle d \rangle_{Pt-Pt}$ (Å)
pristine	-1.13 (-1.63)	-12.07 (-13.12)	2.14 (2.07)	2.60 (2.62)
vacancy	-7.27 (-5.51)	-10.22 (-11.69)	1.97 (1.99)	2.61 (2.59)
divacancy	-7.06 (-9.26)	-10.37 (-13.80)	2.03 (1.99)	2.53 (2.58)
5-8-5	-6.01 (-7.4)	-10.17 (-13.59)	2.01 (2.04)	2.49 (2.52)
555-777	-5.33 (-3.35)	-9.23 (-10.43)	2.04 (2.10)	2.47 (2.50)

^aEP values are in parentheses.

to the other Pt atoms. The 5-8-5 defect reconstruction is broken by

the Pt trimer. The cluster is now an inverted triangle, with one atom bound at a cross configuration while the other two Pt atoms occupy on-top sites. This configuration is higher in energy than the trimer–divacancy configuration and represents a local minimum en route to the latter structure. At the 555-777 defect, the cluster is bound most strongly to the central C atom at only one vertex with a Pt–C bond length equal to 2.04 Å and adopts a tilted configuration with respect to the basal plane. As before, the empirical potential reverses the energetic ordering of binding at the vacancy and divacancy.⁶¹ Finally, all

structures are thermodynamically stable with respect to their individual components.

III.D. Adsorption of Pt Tetramers. For the Pt tetramer (Pt_4), we examined the planar and tetrahedral pyramidal structures shown in Figure 1. Adsorption and formation energies and average C–Pt and Pt–Pt bond lengths for the most stable structures are reported in Table 4, and the corresponding atomic structures (from DFT) are displayed in Figure 6. Although the planar structure is energetically preferred in the gas phase (in agreement with ref 34) by 13 meV/atom, the tetrahedral geometry is most strongly adsorbed on pristine graphene (as was also found in ref 24). The same situation prevails at a

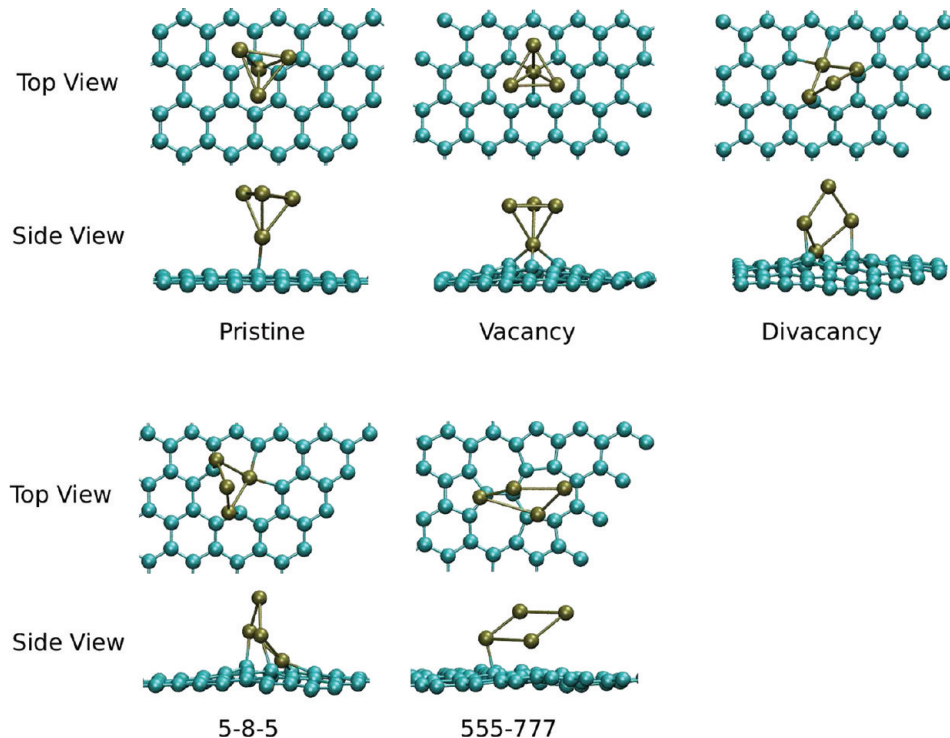


Figure 6. Low-energy DFT configurations for Pt tetramers on graphene. Cyan and gold spheres represent C and Pt atoms, respectively.

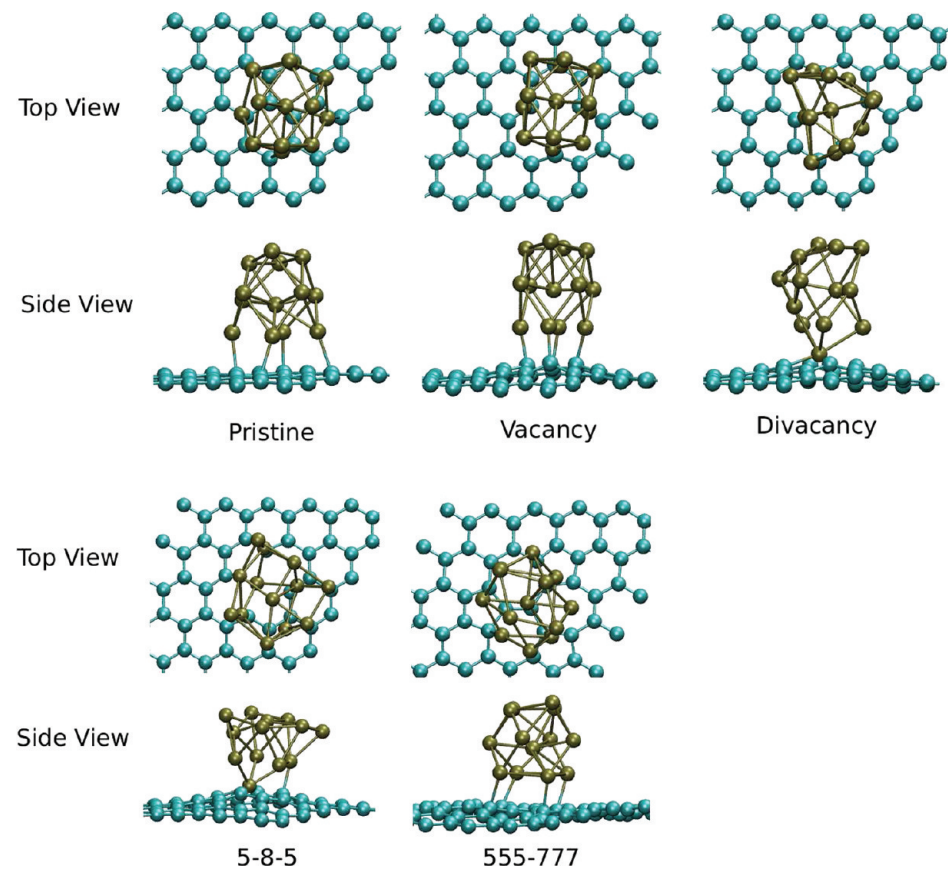


Figure 7. Low-energy configurations obtained by DFT structural relaxation of Pt_{13} clusters on graphene. Cyan and gold spheres represent C and Pt atoms, respectively.

vacancy, where the cluster binds as an inverted tetrahedron with one vertex occupying the same position as the missing C atom, albeit with an out-of-plane displacement as in the

previous cases. When adsorbed at the divacancy and the 5-8-5 reconstruction, the cluster is more like a buckled rhombus with one vertex occupying a cross configuration and two other

Table 5. Optimal Adsorption Energies, Formation Energies, and Average Pt–Pt Bond Lengths ($\langle d \rangle_{\text{Pt–Pt}}$) for Pt_{13} Clusters on Pristine Graphene, Single Vacancy, Unreconstructed Divacancy, 5-8-5 Reconstructed Divacancy, and 555-777 Reconstructed Divacancy for Both Structural Relaxation of High-Symmetry Clusters and Annealed and Relaxed Clusters^a

substrate	relaxation alone			annealing + relaxation		
	E_{ad} (eV)	E_f (eV)	$\langle d \rangle_{\text{Pt–Pt}}$ (Å)	E_{ad} (eV)	E_f (eV)	$\langle d \rangle_{\text{Pt–Pt}}$ (Å)
pristine	0.25 (-3.11)	-49.18 (-54.67)	2.59 (2.61)	-0.84 (-3.72)	-49.96 (-55.20)	2.57 (2.53)
vacancy	-4.67 (-5.86)	-44.64 (-52.48)	2.58 (2.56)	-7.29 (-7.84)	-48.32 (-55.14)	2.56 (2.56)
divacancy	-6.59 (-9.58)	-48.50 (-54.89)	2.59 (2.58)	-7.28 (-10.20)	-49.07 (-55.67)	2.57 (2.59)
5-8-5	-6.28 (-7.33)	-49.03 (-54.30)	2.55 (2.56)	-6.56 (-8.09)	-49.31 (-55.36)	2.55 (2.54)
555-777	-2.07 (-4.66)	-44.40 (-50.93)	2.58 (2.59)	-2.79 (-5.85)	-45.20 (-53.15)	2.55 (2.55)

^aEP results are in parentheses; for annealing + relaxation, the EP energies and bond lengths are averaged over eight different low-energy structures.

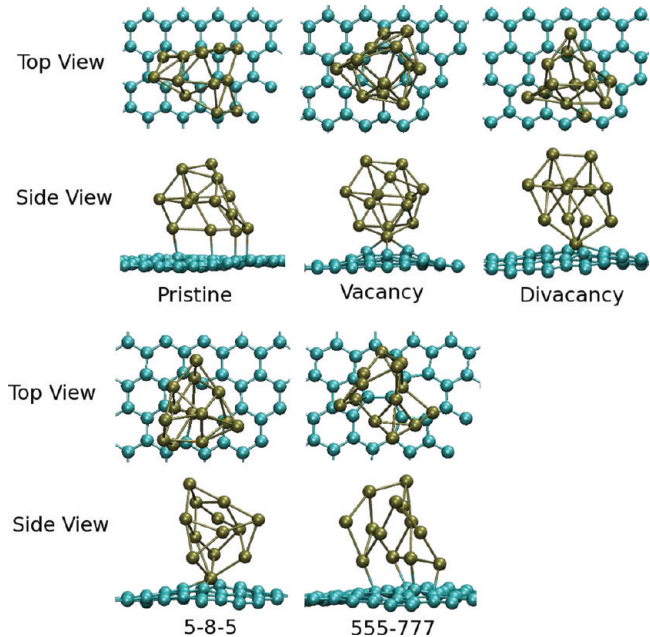


Figure 8. Selected low-energy configurations obtained by DFT structural relaxation of EP-based MD annealing of Pt_{13} clusters on graphene. Cyan and gold spheres represent C and Pt atoms, respectively.

atoms occupying on-top sites. Note that the divacancy and 5-8-5 structures in Figure 6 are simply rotated by approximately 90°

with respect to each other. The 5-8-5 reconstruction is once again broken by the cluster, although this time the system does not seem to fall into a local minimum en route to the tetramer–divacancy configuration. At the 555-777 defect, the cluster resembles a buckled rhombus, although the buckling is less severe than in the divacancy and 5-8-5 cases. The tetramer is bound at only one vertex to the centermost C atom of the 555-777 reconstruction. Once again, the empirical potential reverses the energetic ordering of binding at the vacancy and divacancy. All structures are thermodynamically stable with respect to their individual components.

The Pt tetramer is particularly interesting, as it presents the smallest cluster size for which there is a nontrivial interplay between cluster morphology and substrate structure. In contrast, the monomer and dimer are relatively trivial cases; the trimer always prefers triangular morphologies over linear ones. The Pt_4 cluster is remarkable in that the adsorbed morphologies are clearly derived from two distinct gas-phase isomers, namely, a planar rhombus and a tetrahedron, the preferred morphology being a function of substrate binding site. These site-dependent morphological preferences could play an important role in determining the catalytic activity of such small clusters.

III.E. Adsorption of Pt_{13} Clusters. Finally, we consider the case of a Pt_{13} cluster, which represents the smallest magic cluster according to the geometric shell model.^{43,44} Among its high-symmetry shapes are the icosahedron (I_h) and the cuboctahedron (O_h). These compact shapes are not global minima though, as has been shown by several authors;^{45–48}

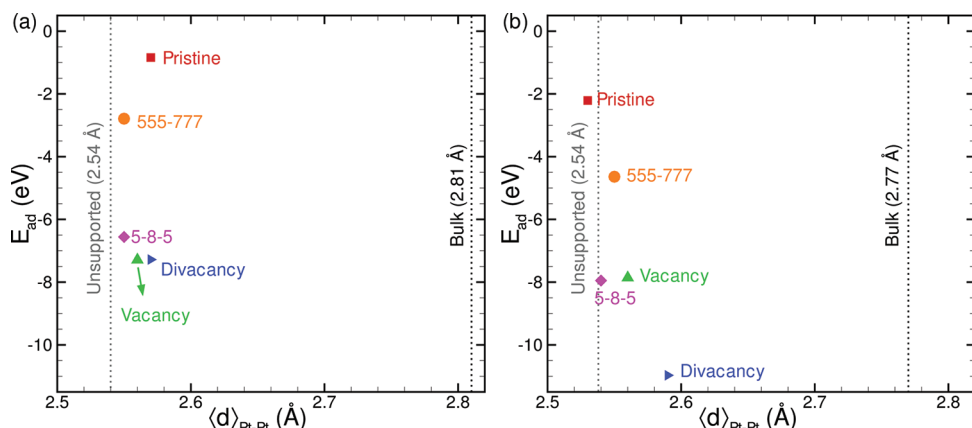


Figure 9. (a) Adsorption energy (E_{ad}) versus average bond length ($\langle d \rangle_{\text{Pt–Pt}}$) from DFT relaxation of the lowest-energy Pt_{13} clusters on graphene supports obtained after EP-based MD annealing. Vertical dotted lines indicate the average bond lengths for bulk Pt and for unsupported clusters (annealed clusters removed from the graphene substrate and relaxed). (b) E_{ad} versus $\langle d \rangle_{\text{Pt–Pt}}$ obtained after averaging over eight different low-energy structures obtained with the EP-based MD annealing schedule. (Error bars are much too small to be visible on this scale and are omitted.) The corresponding data are in Table 5.

instead, there exist several low-symmetry, open structures that are more energetically preferred. The task of systematically finding low-energy isomers is already a computationally tedious one for unsupported clusters, let alone supported ones. Rather than attempting to comprehensively catalog low-energy supported clusters, we simply examine a few structures obtained here from MD annealing and contrast these with local minima obtained for the adsorption of high-symmetry structures.

First, I_h and O_h clusters were introduced in the vicinity of the graphene sheet, and the total energy was minimized using a conjugate gradient algorithm so as to find a local minimum. Planar clusters were already shown by Okazaki-Maeda et al.²⁴ to be energetically unfavorable and are not considered here. (Test calculations were essentially in agreement with that work.) The clusters were introduced at different orientations with respect to the sheet (e.g., with a triangular or square face parallel to the sheet, a vertex closest to the sheet, and so on). The lowest-energy structures that were obtained from energy minimization with DFT are displayed in Figure 7; adsorption and formation energies are reported in Table 5. As seen from these data, the Pt clusters bind most strongly to the unreconstructed divacancy, followed by the 5-8-5 defect. The latter once again unreconstructs upon cluster adsorption. We note that for these two cases, the initial structure of the cluster was icosahedral, but the relaxed structure bears little resemblance to an icosahedron (see Figure 7), unlike the relaxed structures on other substrates where there is some resemblance to the starting structure (I_h or O_h as appropriate). Thus, even structural relaxation to a local minimum in the presence of certain substrate defects can induce severe morphological changes in the cluster. We also note that the DFT and EP data are now in qualitative agreement with respect to the relative ordering of adsorption energies. This gives us some confidence in using EP calculations as a preliminary step to generate low-energy candidates for additional investigation with DFT.

Thereafter, we took the relaxed clusters and subjected them to an MD annealing schedule as described in section II. Some of the morphologies of the clusters obtained from this procedure are displayed in Figure 8; the adsorption and formation energies after annealing and relaxation are reported in Table 5. There are other near-degenerate structures that are not displayed here but were taken into account in constructing the plot of adsorption energy versus average Pt–Pt bond length in Figure 9 (discussed further below).

It is immediately apparent that the clusters bear no resemblance to their high-symmetry I_h or O_h counterparts. Instead, these are low-symmetry, open shapes that are more strongly adsorbed (by several electronvolts in some cases) and are thermodynamically more stable than the structures obtained from relaxation alone. The vacancy and the unreconstructed divacancy are seen to be the strongest binding defects, differing by only 0.01 eV in their binding energies. Interestingly, for both the vacancy and divacancy, the cluster has one vertex atom in a near-substitutional or cross configuration, respectively. The rest of the cluster is supported on this basal atom, leaving a large number of undercoordinated Pt atoms. For the other cases, in contrast, there are more Pt–C bonds, consequently, with fewer undercoordinated Pt atoms. The number of undercoordinated surface atoms is directly related to the number of active surface sites for catalytic reactions. Thus, these results establish one possible effect at the morphological level of the substrate defect

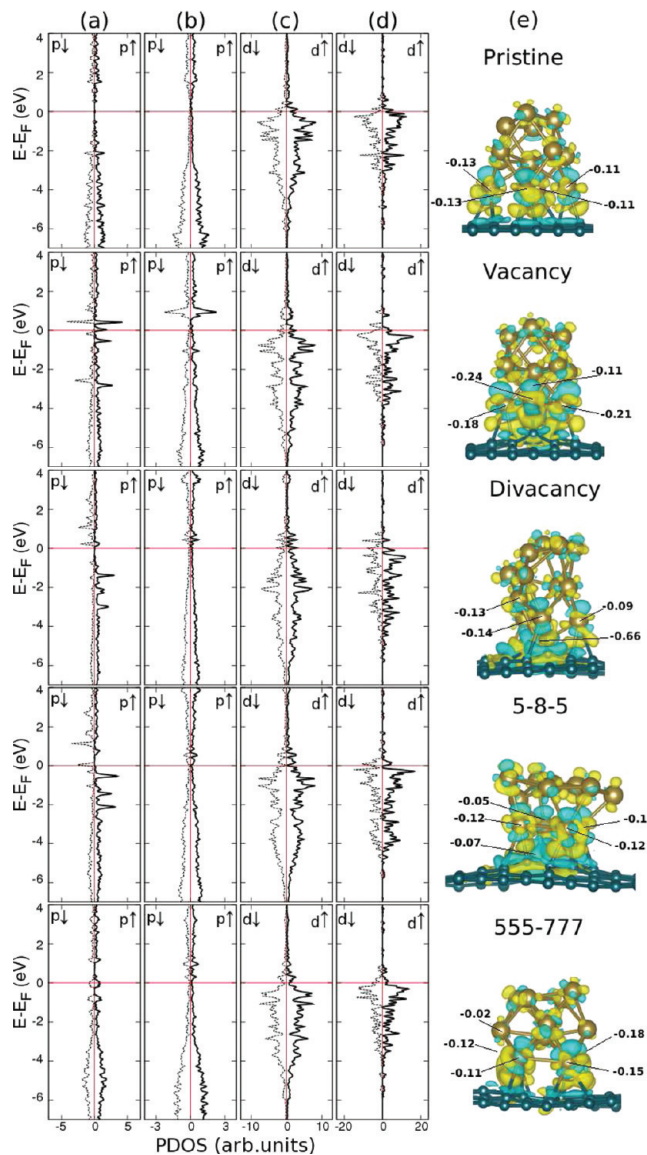


Figure 10. Projected density of states (PDOS) plots for clusters subjected to relaxation alone: (a) free graphene, (b) graphene after Pt₁₃ adsorption, (c) adsorbed Pt₁₃ cluster, (d) free Pt₁₃ cluster. (e) Charge-density difference plots. (Isosurfaces are at 0.027 e/Å³); yellow (blue) color represents charge accumulation (depletion). The charge lost by Pt atoms bound to the substrate is indicated.

on potential catalytic activity of the cluster, namely, controlling the extent of undercoordination of Pt atoms.

To quantify the morphological changes in the low-symmetry clusters, we display in Figure 9 the adsorption energy versus the average Pt–Pt bond length of the Pt₁₃ clusters adsorbed on the five different graphene substrates. The average bond lengths for bulk Pt and the unsupported clusters are also indicated in the figure; the smaller average bond length in the latter case is to be expected because of the significant degree of undercoordination of Pt atoms in these small clusters as compared to bulk Pt. The DFT data (Figure 9a) are from relaxation of the lowest-energy structures obtained from the initial EP-based MD annealing step; the EP data (Figure 9b) were obtained by averaging⁶² over eight different low-energy configurations sampled over the course of the annealing schedule. One can see from Figure 9 that the supported clusters all have slightly larger average bond

lengths than the unsupported ones. We attribute this difference to the formation of Pt–C bonds, which decreases the degree of undercoordination of at least a few Pt atoms. We do not have sufficient statistics from DFT calculations to make a conclusive connection between the average Pt–Pt bond length and the binding energy as a function of substrate defect although it would seem from the data that larger binding energies (more negative E_f) correlate with larger average Pt–Pt bond lengths. The EP data, which were obtained by averaging over a few different low-energy configurations, do seem to offer a more conclusive corroboration of this trend. In related work on adsorption of Pt_{100} clusters on edges of carbon platelets, Sanz-Navarro et al.³⁵ showed that Pt clusters tend to lose their initial partial fcc-like structure upon adsorption; this is accompanied by an increase in the average bond length of the adsorbed cluster by 1.4% over that of a free cluster. Previous DFT calculations of CO oxidation on Pt(111) surfaces have demonstrated the profound influence of lattice strain on reaction enthalpies and kinetics, with the potential to even change the rate-limiting step in the reaction network.⁵⁷ We expect that such effects could also be operative here, with the substrate defect (rather than a macroscopic externally applied strain field) influencing the extent of strain in the cluster bonds.

Table 6. d-Band Centers (ϵ_d) of Adsorbed Pt_{13} Clusters (Relative to the Fermi Level) on Various Defective and Defect-Free Graphene Supports and Charge Transfer (Δq) from the Pt_{13} Cluster to the Support^a

substrate	ϵ_d (eV)		Δq (e)	
	relaxation alone	annealing + relaxation	relaxation alone	annealing + relaxation
pristine	-2.30	-2.34	-0.18	-0.08
vacancy	-2.36	-2.53	-0.35	-0.48
divacancy	-2.54	-2.49	-0.71	-0.81
5-8-5	-2.60	-2.58	-0.79	-0.72
555-777	-2.36	-2.51	-0.29	-0.30

^aElectron charge taken to be negative.

III.F. Electronic Structure of Adsorbed Pt_{13} Clusters.

Having investigated the binding energetics and structural morphology of Pt_{13} clusters adsorbed on pristine and defective graphene, we now turn our attention to the electronic structure of these adsorbed clusters. The electronic structure of smaller Pt_n ($n = 1, 2, 3, 4$) clusters has been studied in detail previously^{30–32, 56, 58} and is not revisited here. The electronic structure of Pt_{13} clusters, on the other hand, has only been considered in situations where the clusters have been relaxed from high-symmetry initial structures;^{21, 27, 36} a detailed comparison with annealed clusters is therefore warranted. In the following, we present a detailed electronic structure analysis based on the projected density of states (PDOS), d-band shifts, and charge transfer for adsorbed clusters subjected to relaxation alone and a combination of annealing and relaxation.

First, we consider the case of graphene-supported Pt_{13} clusters, which were obtained by relaxation from initial high-symmetry shapes (Figure 7). The total density of states (DOS) was projected on to the p orbitals of C atoms and d orbitals of Pt atoms at the support–cluster interface that are involved in bond formation. The summed p and d DOS for these C and Pt atoms are displayed in Figures 10b and 10c, respectively. To facilitate an understanding of how the p and d states are modified upon cluster adsorption, the p and d DOS from the same atoms in the isolated graphene support and cluster are displayed in Figures 10a and 10d, respectively. By comparing Figures 10c and 10d for the various cases, it is immediately apparent that the Pt d-band undergoes significant broadening upon cluster adsorption; the occupied d states, which were confined to an energy range of 4 eV below the Fermi level are now clearly visible up to about 7 eV below the Fermi level. At the same time, the sharp peaks in the vicinity of the Fermi level in Figure 10a, arising from dangling C bonds at various point defects, disappear upon adsorption of the Pt cluster as seen in Figure 10b accompanied by an overall broadening of the p DOS; for the pristine support, where there are no dangling bonds, there is merely an overall broadening of occupied C p states upon cluster adsorption. These observations are a clear sign of bond formation between the Pt cluster and the support.

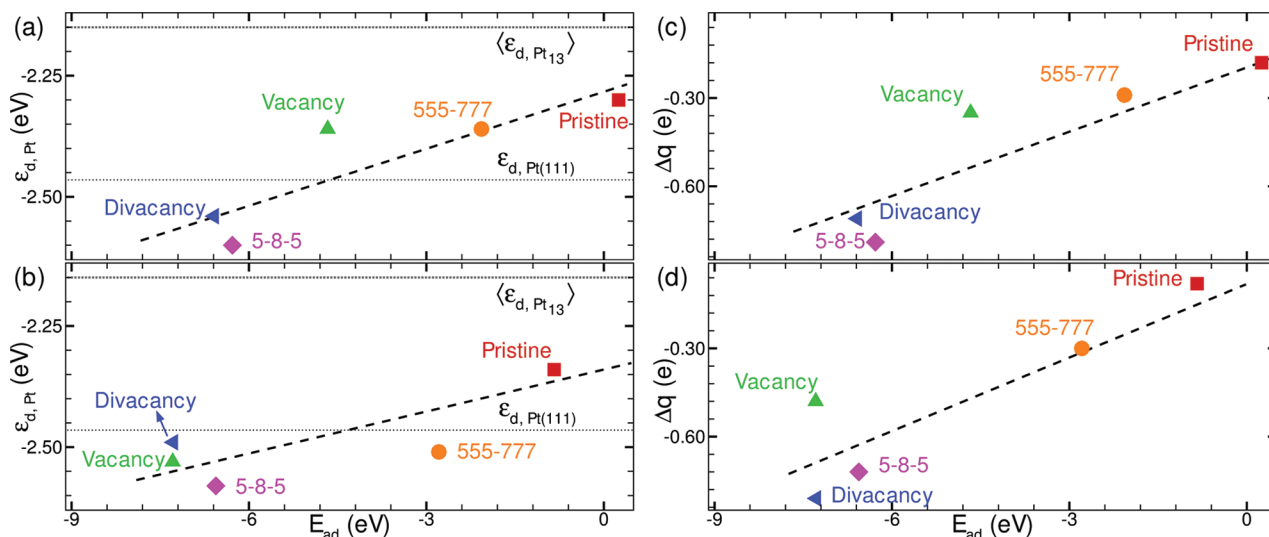


Figure 11. Position of d-band center ($\epsilon_{d,\text{Pt}}$) relative to the Fermi level for supported Pt_{13} clusters subjected to (a) relaxation alone and (b) annealing followed by relaxation. Horizontal dotted lines indicate the d-band center of the $\text{Pt}(111)$ surface ($\epsilon_{d,\text{Pt}(111)}$) and the average d-band center of the various free Pt_{13} clusters ($\langle \epsilon_{d,\text{Pt}13} \rangle$) considered here. Charge transfer from (c) relaxed and (d) annealed and relaxed Pt_{13} clusters to the substrate. (The electron charge is taken to be negative here.) The dashed lines in all plots are merely guides to the eye.

This is further supported by the charge-density difference plots in Figure 10e, which show significant redistribution of charge in the vicinity of the support–cluster interface.

A more quantitative analysis of the charge transfer to the support as well as the shifts in the cluster d band is also possible. To quantify the total charge transfer, a Bader analysis^{59,60} was performed on the final structure (cluster + support). This procedure partitions the total charge density between atoms; by summing the final charge density over the Pt₁₃ cluster and the support atoms and comparing with the initial number of electrons in the cluster and support, we consistently find an appreciable net charge transfer from the Pt₁₃ cluster to the graphene support (defective or otherwise). As seen from these charge-transfer data, displayed in Table 6 and Figure 11c, the stronger the binding of the cluster to the support the greater the charge transferred to the support. The shifts in the Pt d band upon adsorption were quantified by determining the position of the d-band center in the adsorbed cluster. The filled d states of all Pt atoms in the cluster were used in this procedure. As seen from the data in Table 6 and Figure 11a, the d-band centers undergo an appreciable downward shift, relative to their average position in the unsupported clusters, upon binding to the support. Once again, there is a positive correlation between the strength of binding and the downward shift of the d-band center. For the clusters with strongest binding (at a divacancy and 5-8-5 defect), the d-band center is shifted even further below that of the Pt(111) surface.

A similar electronic structure analysis was performed for the clusters that were first subjected to MD annealing followed by DFT structural relaxation (Figure 8). Partial density of states plots and charge density difference plots for this case are displayed in Figure 12; the overall features qualitatively follow the discussion above. There is a broadening of the Pt d and C p bands, disappearance of sharp localized states near the Fermi level, and significant redistribution of charge at the cluster-support interface. There is, once again, transfer of electrons from the Pt₁₃ cluster to the support and a downshift of the Pt d-band center upon adsorption. The extent of charge transfer and downshift of the d band are positively correlated with the binding energy of the cluster (Table 6; Figure 11b,d). For all the cases of binding to defective supports, the d-band center is seen to shift below that of a Pt(111) surface.

The case of binding to the vacancy defect is particularly interesting. We recall that the Pt₁₃ cluster has an adsorption energy of -4.67 eV when relaxed from a high-symmetry structure, which is significantly higher (weaker binding) than the adsorption energy of -7.29 eV found after the annealing procedure (Table 5): the latter structure being more strongly adsorbed, the d-band center is noticeably lowered (by 0.17 eV) relative to the former. Similarly, the annealed and relaxed structure transfers an additional 0.13 electrons to the support relative to the relaxed high-symmetry structure. This example underscores the need to search more extensively for low-symmetry, low-energy isomers of supported clusters when trying to make computational predictions of their catalytic activity. We also note that these observations of charge transfer from the Pt cluster to the graphene support accompanied by a shift of the Pt d band away from the Fermi level in the presence of a vacancy are consistent with previous reports.^{29–31,36}

The data for binding to divacancies and divancy reconstructions reported here essentially complete the picture of binding of small Pt clusters to point defects in graphene. Overall, from the positions of the d-band centers in Table 6 and Figure 11, we

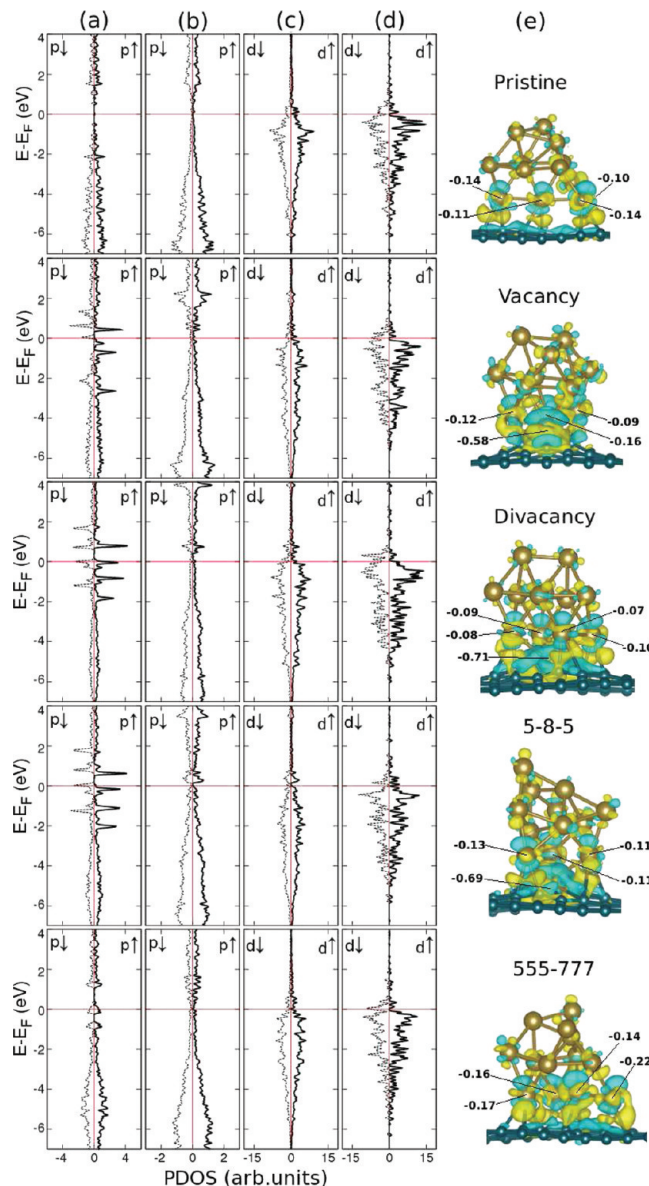


Figure 12. Projected density of states (PDOS) plots for annealed and relaxed clusters: (a) free graphene, (b) graphene after Pt₁₃ adsorption, (c) adsorbed Pt₁₃ cluster, (d) free Pt₁₃ cluster. (e) Charge-density difference plots. (Isosurfaces are at 0.034 e/Å³); yellow (blue) color represents charge accumulation (depletion). The charge lost by Pt atoms bound to the substrate is indicated.

conclude that point defects in graphene lower the d-band center of Pt₁₃ clusters below that of a Pt(111) surface (and significantly below that of unsupported clusters). This lowering of the d-band center is expected to decrease the binding energy of CO molecules, among others, which provides a plausible explanation for experimental observations of increased CO tolerance^{5,6} exhibited by reduced graphene oxide-Pt nanocomposites. We defer actual calculations of CO binding to these supported clusters to future work. Additionally, studies of the role of functional groups present on reduced graphene oxide in cluster adsorption are also deferred to future work.

IV. CONCLUSIONS

We investigated the binding energetics and morphology of low-energy structures of Pt nanoclusters on defect-free and

defective graphene substrates, using a combination of DFT and bond-order potential simulations. The primary conclusions of our study are as follows:

- (1) Point defects and their reconstructions in graphene act as strong binding traps for Pt clusters. Over the range of cluster sizes studied here, these defects bind Pt clusters more strongly than pristine graphene by several electron-volts. Unreconstructed defects tend to be the strongest binding traps, although reconstructed defects can also serve as fairly strong traps. These observations provide a plausible explanation for the long-term stability toward sintering observed in Pt–graphene composites;^{5–7} the graphene support in these composites is derived from graphene oxide, which is prone to defects.^{14–16} Furthermore, the existence of defects in the graphene support could also provide an explanation for the greater stability toward sintering observed in Pt–graphene composites relative to Pt–carbon nanotube composites.⁶ Thus, inducing pre-existing point defects in graphene supports could provide a facile route for synthesizing robust carbon-supported Pt nanocatalysts.
- (2) By employing a combination of empirical-potential-based simulated annealing and DFT calculations, we have unambiguously shown that supported Pt clusters are neither high-symmetry structures nor readily derived from high-symmetry structures, as is often the assumption made in computational modeling. Instead, small clusters tend to adopt more open, low-symmetry morphologies similar to those observed in previous DFT studies of annealing of clusters in a vacuum.^{45–48} Even though clusters that are nominally of high symmetry in their initial state can undergo severe structural distortion upon relaxation and binding to a defect in the graphene support, their annealed, low-symmetry counterparts are consistently lower in energy, sometimes by *several* electronvolts. These observations suggest that future investigations should first focus on determining at least a few candidate low-energy structures before addressing issues related to the catalytic activity of clusters. Without this initial step, the structures being sampled could simply be ones that are stuck in higher metastable minima, which could, in turn, corrupt further inferences related to binding energetics of molecules and energy barriers for reactions on the cluster.
- (3) The formation of strong bonds with the carbon substrate potentially influences the strain in a cluster: within the limited statistics available here, the average Pt–Pt bond length appears to increase with stronger binding to the substrate. We expect that this effect is of greater relevance for the small clusters considered here and this additional strain (or strain relief with respect to the bulk) in the bonds could affect the activity of the cluster. More comprehensive studies over several different cluster sizes are needed to make this connection clearer.
- (4) Electronic structure studies reveal a clear tendency for charge transfer from Pt clusters to the graphene substrate. Within the limited statistics available here, it would appear that there is a positive correlation between the strength of binding to the defect and the extent of charge transferred. Similarly, stronger binding of the cluster to the substrate appears to lead to a greater downshift of the cluster d-band center; in several instances, the cluster d-band center shifts further below that of a Pt(111) surface. This result suggests

a decrease in the binding energy of CO to Pt clusters bound at point defects, which could offer a plausible explanation for reports^{5,6} of enhanced CO tolerance of reduced graphene oxide-supported Pt nanoclusters. Although this downshift in the d-band center might be desirable for inhibiting catalyst poisoning, it should be noted that the concomitant decrease in binding energy of other molecular species might adversely impact the ability of the Pt clusters to catalyze reactions, which requires further investigation.

■ AUTHOR INFORMATION

Corresponding Author

*E-mail: ashwin@engin.umass.edu.

Notes

The authors declare no competing financial interest.

■ ACKNOWLEDGMENTS

We gratefully acknowledge startup support from the University of Massachusetts Amherst.

■ REFERENCES

- (1) Auer, E.; Freund, A.; Pietsch, J.; Tacke, T. *Appl. Catal. A: Gen.* **1998**, *173*, 259.
- (2) Planeix, J. M.; Coustel, N.; Coq, B.; Brotons, V.; Kumbhar, P. S.; Dutartre, R.; Geneste, P.; Bernier, P.; Ajayan, P. M. *J. Am. Chem. Soc.* **1994**, *116*, 7935.
- (3) Tang, H.; Chen, J. H.; Nie, L. H.; Liu, D. Y.; Deng, W.; Kuang, Y. F.; Yao, S. Z. *J. Colloid Interface Sci.* **2004**, *269*, 26.
- (4) Kongkanand, A.; Kuwabata, S.; Girishkumar, G.; Kamat, P. *Langmuir* **2006**, *22*, 2392.
- (5) Yoo, E.; Okata, T.; Akita, T.; Kohyama, M.; Nakamura, J.; Honma, I. *Nano Lett.* **2009**, *9*, 2255.
- (6) Li, Y.; Gao, W.; Ci, L.; Wang, C.; Ajayan, P. M. *Carbon* **2010**, *48*, 1124.
- (7) Kou, R.; Shao, Y.; Wang, D.; Engelhard, M. H.; Kwak, J. H.; Wang, J.; Viswanathan, V. V.; Wang, C.; Lin, Y.; Wang, Y.; Aksay, I. A.; Liu, J. *Electrochem. Commun.* **2009**, *11*, 954.
- (8) Seger, B.; Kamat, P. V. *J. Phys. Chem. C* **2009**, *113*, 7990.
- (9) Zhong, J.; Nackashi, D.; Lu, W.; Kittrell, C.; Tour, J. M. *Chem. Mater.* **2010**, *22*, 5695.
- (10) Gan, Y.; Sun, L.; Banhart, F. *Small* **2008**, *4*, 587.
- (11) Morrow, B. H.; Striolo, A. *Nanotechnology* **2008**, *19*, 195711.
- (12) Rodriguez-Manzo, J. A.; Cretu, O.; Banhart, F. *ACS Nano* **2010**, *4*, 3422.
- (13) Zoval, J. V.; Lee, J.; Gorer, S.; Penner, R. M. *J. Phys. Chem. B* **1998**, *102*, 1166.
- (14) Li, J. L.; Kudin, K. N.; McAllister, M. J.; Prud'homme, R. K.; Aksay, I. A.; Car, R. *Phys. Rev. Lett.* **2006**, *96*, 176101.
- (15) Paci, J. T.; Belytschko, T.; Schatz, G. C. *J. Phys. Chem. C* **2007**, *111*, 18099.
- (16) Bagri, A.; Mattevi, C.; Acik, A.; Chabal, Y. J.; Chhowalla, M.; Shenoy, V. B. *Nat. Chem.* **2010**, *2*, 581.
- (17) Kou, R.; Shao, Y.; Mei, D.; Nie, Z.; Wang, D.; Wang, C.; Viswanathan, V. V.; Park, S.; Aksay, I. A.; Lin, Y.; Wang, Y.; Liu, J. *J. Am. Chem. Soc.* **2011**, *133*, 2541.
- (18) Vedala, H.; Sorescu, D. C.; Kotchey, G. P.; Star, A. *Nano Lett.* **2011**, *11*, 2342.
- (19) Acharya, C. K.; Turner, C. H. *Surf. Sci.* **2008**, *602*, 3595.
- (20) Acharya, C. K.; Sullivan, D. I.; Turner, C. H. *J. Phys. Chem. C* **2008**, *112*, 35.
- (21) Kim, G.; Jhi, S.-H. *ACS Nano* **2011**, *5*, 805.
- (22) Acharya, C. K.; Sullivan, D. I.; Turner, C. H. *J. Phys. Chem. C* **2008**, *112*, 13607.
- (23) Maiti, A.; Ricca, A. *Chem. Phys. Lett.* **2004**, *395*, 7.
- (24) Okazaki-Maeda, K.; Morikawa, Y.; Tanaka, S.; Kohyama, M. *Surf. Sci.* **2010**, *604*, 144.

- (25) Dai, X.-Q.; Tang, Y.-N.; Zhao, J.-H.; Dai, Y.-W. *J. Phys.: Condens. Matter* **2010**, *22*, 31.
- (26) Akturk, O. U.; Tomak, M. *Phys. Rev. B* **2009**, *80*, 8.
- (27) Cuong, N. T.; Fujiwara, A.; Mitani, T.; Chi, D. H. *Comput. Mater. Sci.* **2008**, *44*, 163.
- (28) Kong, K.; Choi, Y.; Ryu, B.-H.; Lee, J.; Chang, H. *Mater. Sci. Eng. C* **2006**, *26*, 1207.
- (29) Okamoto, Y. *Chem. Phys. Lett.* **2006**, *420*, 382.
- (30) Wang, J.; Lv, Y.; Li, X.; Dong, M. *J. Phys. Chem. C* **2009**, *113*, 890.
- (31) Chi, D. H.; Cuong, N. T.; Tuan, N. A.; Kim, Y.-T.; Bao, H. T.; Mitani, T.; Ozaki, T.; Nagao, H. *Chem. Phys. Lett.* **2006**, *432*, 213.
- (32) Cuong, N. T.; Sugiyama, A.; Fujiwara, A.; Mitani, T.; Chi, D. H. *Phys. Rev. B* **2009**, *79*, 23.
- (33) Cabria, I.; Lopez, M. J.; Alonso, J. A. *Phys. Rev. B* **2010**, *81*, 3.
- (34) Błoński, P.; Hafner, J. *J. Chem. Phys.* **2011**, *134*, 154705.
- (35) Sanz-Navarro, C. F.; Åstrand, P.-O.; Chen, D.; Rønning, M.; van Duin, Adri C. T.; Jacob, T.; Goddard, W. A. III. *J. Chem. Phys. A* **2008**, *112*, 1392.
- (36) Lim, D.-H.; Wilcox, J. *J. Phys. Chem. C* **2011**, *115*, 22742.
- (37) Zhou, M.; Zhang, A.; Dai, Z.; Zhang, C.; Feng, Y. P. *J. Chem. Phys.* **2010**, *132*, 194704.
- (38) Logsdail, A. J.; Akola, J. *J. Phys. Chem. C* **2011**, *115*, 15240.
- (39) Lim, D.-H.; Negreira, A. S.; Wilcox, J. *J. Phys. Chem. C* **2011**, *115*, 8961.
- (40) Liu, X.; Li, L.; Meng, C.; Han, Y. *J. Phys. Chem. C* **2012**, *116*, 2710.
- (41) Lee, G.-D.; Wang, C. Z.; Yoon, E.; Hwang, N.-M.; Kim, D. Y.; Ho, K. M. *Phys. Rev. Lett.* **2005**, *95*, 205501.
- (42) Lee, G.-D.; Wang, C. Z.; Yoon, E.; Hwang, N.-M.; Ho, K. M. *Phys. Rev. B* **2006**, *74*, 245411.
- (43) Baletto, F.; Ferrando, R. *Rev. Mod. Phys.* **2005**, *77*, 371.
- (44) Solov'yov, I.; Solov'yov, A.; Greiner, W.; Koshelev, A.; Shutovitch, A. *Phys. Rev. Lett.* **2003**, *90*, 053401.
- (45) Wang, L.-L.; Johnson, D. D. *Phys. Rev. B* **2007**, *75*, 235405.
- (46) Kumar, V.; Kawazoe, Y. *Phys. Rev. B* **2008**, *77*, 2532.
- (47) Longo, R.; Gallego, L. *Phys. Rev. B* **2006**, *74*, 193409.
- (48) Chang, C.; Chou, M. *Phys. Rev. Lett.* **2004**, *93*, 133401.
- (49) Kresse, G.; Furthmüller, J. *Comput. Mater. Sci.* **1996**, *6*, 15; *Phys. Rev. B* **1996**, *54*, 11169.
- (50) Blöchl, P. E. *Phys. Rev. B* **1994**, *50*, 17953.
- (51) Kresse, G.; Joubert, D. *Phys. Rev. B* **1999**, *59*, 1758.
- (52) Perdew, J. P.; Burke, K.; Ernzerhof, M. *Phys. Rev. Lett.* **1996**, *77*, 3865.
- (53) Methfessel, M.; Paxton, A. T. *Phys. Rev. B* **1989**, *40*, 3616.
- (54) Plimpton, S. *J. J. Comput. Phys.* **1995**, *117*, 1.
- (55) Albe, K.; Nordlund, K.; Averback, R. S. *Phys. Rev. B* **2002**, *65*, 195124.
- (56) Krasheninnikov, A. V.; Lehtinen, P. O.; Foster, A. S.; Pyykkö, P.; Nieminen, R. M. *Phys. Rev. Lett.* **2009**, *102*, 126807.
- (57) Grabow, L.; Xu, Y.; Mavrikakis, M. *Phys. Chem. Chem. Phys.* **2006**, *8*, 3369.
- (58) Tang, Y.; Yang, Z.; Dai, X. *J. Chem. Phys.* **2011**, *135*, 224704.
- (59) Bader, R. F. W. *Chem. Rev.* **1991**, *91*, 893.
- (60) Henkelman, G.; Arnaldsson, A.; Jónsson, H. *Comput. Mater. Sci.* **2006**, *36*, 254.
- (61) This discrepancy from the EP calculation persists even in tests on much larger graphene sheets (1500 atoms) suggesting deficiencies in the potential itself; size effects can be conclusively ruled out.
- (62) The energies $E_{C_m+Pt_n}$ and E_{Pt_n} should be replaced by their averages in eqs 1 and 2.